Locating of The Jacket Type Offshore Wind Turbine with Tuned Liquid Column Gas Damper for Iranian Shores

Mohammad Hossein Jahangir [1,*], Saba Nasiri [1], and Shamsodin Tajik [1]

[1] *Faculty of New Sciences and Technologies, University of Tehran, Tehran, Iran*
**Corresponding author: mh.jahangir@ut.ac.ir*

Manuscript received 07 January, 2024; revised 16 September, 2024; accepted 18 September, 2024. Paper no. JEMT- 2401-1484.

This study investigates the optimal installation sites for offshore wind turbines along Iran's shores, emphasizing the use of renewable wind energy in response to fossil fuel pollution and energy shortages. Given the high wind potential along these shores, the study specifically examines the use of a jacketed-type offshore wind turbine with a Tuned Liquid Column Gas Damper (TLCGD) to mitigate wind and wave vibrations, thereby reducing potential damage. The research involved analyzing data from 26 oceanographic stations and running simulations in MATLAB with 10,000 wave and wind scenarios to assess hydrodynamic and aerodynamic forces on the turbine model. The primary goal was to find locations with minimal fluid displacement in the TLCGD system and maximum power generation capacity. The study's findings highlight that in the Caspian Sea, the most suitable installation sites are at coordinates (37.0 N, 53.2 E) with a power output of 3.8 MW and 45 cm displacement, (38.0 N, 49.4 E) with 4.5 MW and 48.7 cm displacement, and (38.4 N, 49.1 E) with 3.5 MW and 46.9 cm displacement. For the Oman Sea, the analysis identified potential sites at (24.8 N, 58.1 E) with 1.7 MW and 43.4 cm displacement, but the overall suitability was compromised due to lower power output and higher displacement. In contrast, the Persian Gulf showed the highest potential, with optimal sites at (28.1 N, 50.1 E) offering 3.9 MW and 49.1 cm displacement, and (27.0 N, 53.0 E) with 4.2 MW and 50 cm displacement. These locations, particularly in the northwest and central regions of the Persian Gulf, were deemed the best for installing this type of wind turbine system.

Keywords: *Offshore Wind Turbine; Tuned Liquid Column-gas Damper; Foundation Displacement; Power Generation; Wave Energy Convertor*

http://dx.doi.org/10.22109/jemt.2024.434477.1484

Nomenclature

W	Vertical Wave Speed (m/s)
V	Speed (m/s)
$\dot{a}$	Total Acceleration (m/s^2)
Z_a	Wave Amplitude (m)
ω	Angular Frequency (rad/s)
U	Acceleration of the Wave (m/s^2)
F_D	Drag Force (N)
F_I	Inertia force (N)
C_d	Drag Coefficient
C_I	Inertia Coefficients
$\dot{u}$	Jacket Absolute Velocity (m/s)
$\ddot{u}$	Absolute Acceleration (m/s^2)
δ_L	Hydraulic Head Drop
K_C	Contraction Coefficients
K_E	Expansion Coefficients
C_p	Coefficient
R_{pd}	Power to displacement ratio

Greek Letters

λ	Area Ratio
ρ_w	Water Density (g/cm3)

Acronyms

TLCGD	Tuned Liquid Column Gas Damper
TMD	Tuned Mass Damper
TLCD	Tuned Liquid Column Damper
AMD	Active Mass Damper
MTMD	Multiple Tuned Mass Dampers
JOWT	Jacket-Type Offshore Wind Turbine
MDOF	Multi-Degree of Freedom

1. Introduction

Nowadays, using renewable energy sources is inevitable regarding population growth [1], increasing demand for energy, and fossil fuel limitations [2]. Wind energy, a prominent alternative [3] , is currently the second-largest renewable energy resource worldwide [4]. Offshore wind turbines, due to their high wind quality and greater energy generation potential, have gained significant interest [5], particularly in areas with limited land availability [6]. Developed countries such as Japan, China, Norway, and the USA have recently industrialized this technology [7]. In this respect, the first floating offshore wind turbines were installed in Norway in 2009, called Hywind [8]. Despite these advantages, offshore wind turbines face challenges, particularly their low structural tolerance to wave and wind-induced vibrations [9], , which can lead to significant damage and high maintenance costs [10, 11]. Larger turbines are especially prone to increased vibrations [12], reducing component lifespan [13] and raising failure risks [14]. Solutions such as constructing flexible turbines [15], and implementing damping systems have been proposed to control these vibrations [16]. Among these, Tuned Liquid Dampers (TLDs) have recently gained attention for their effectiveness in vibration mitigation [17].

Based on the damping operating mechanism, these controlling systems are divided into three categories: active, quasi-active, and passive [18, 19]. The tuned mass damper (TMD), tuned liquid column damper (TLCD), and active mass damper (AMD) are among the most important damping systems [20]. In this type of damper, feedback from turret displacement and damper mass relative velocity is used to control additional actuator forces [21, 22]. The damping effect of the multiple tuned mass dampers (MTMD) were studied by Dinh VN & Basu (2015) [23]. Both experimental and numerical studies have shown that the application of TMD to offshore wind turbines is efficient [24]. Zhang et al. (2023) [25] found that Tuned Mass Dampers (TMDs) perform best when the offshore wind turbine (OWT) is parked, significantly reducing structural vibrations, with optimal reductions of 25.41% in displacement and 24.76% in acceleration. Zhang et al. (2024) [26] found that Tuned Mass Dampers (TMDs) reduced peak acceleration by 7.8% and bending moments by 8.8% in Floating Offshore Wind Turbines (FOWTs), enhancing their structural safety. In this regard, TLCGD is the newest and more practical control system, which is used to reduce the wind (aerodynamic) and the waves (hydrodynamic) vibrations that occur when moving and bending the structure. Such systems significantly prolong wind turbines' fatigue life (Nf) [27]. TLCGD system is investigated in detail by Cowell et al.[12]. As TLCD, TLCGD is a U-shaped container full of water with its vertical section filled with compressed gas and its top sealed [28]. The system is a U-shaped steel pipe filled with water up to the half section and can minimize a large amount of kinetic energy posed to the system [29]. When the energy exerted is transmitted from the system to TLCGD, the liquid moves in the pipes and terminates the vibrations throughout the upper structure along the parallel lines to the liquid and gravity recovering forces [30]. Therefore, this system is also called an anti-rotation tank or U-shaped tank. According to Coudurier et al., the performance of TLCGD can reduce vibrations by 39% [31].

Carrier & Miles (1960) used a ring-type system to control and minimize the space satellite fluctuations. Also, Balendra et al. investigated the effects of TLCD on suppressing accelerations due to the wind for waves with natural frequency [32]. Gao & Kwok (1987) proposed different geometrical form systems such as cylinder cube, cone, and U-shape to optimize this system [33]. In another study, Vandiver & Mitome examined the effects of the system in responding to the marine structures under wind loading and introduced the vibration minimization effects [34]. Yamamoto & Kawahara (1999) investigated the effects of the TLCGD system behavior against vibrations and wave structure [35]. In addition, the optimal values and parameters of designing for TLCGD under the sonic wave's effect were investigated by yalla & Kareem (2000) [36]. Based on Dezvareh, Bargi, and Mousavi's modeling, this type of control and vibration absorption system is defined as passive [37].

Depending on wind velocity and wave energy, the TLCGD system can reduce the vibrations in offshore wind turbines on nozzle up to 45-51% [16]. Sathish and Sahithp introduced the latest version of the TLCGD system [38]. The TLCGD system uses internal liquid to balance the structure's frequency and reduce force, offering high flexibility and responsiveness [39]. Ahmad et al. found that an active control strategy improved the reliability and survival of tension foundation platforms under wind and wave loads, significantly reducing TKP movement [18]. As soil properties vary, so do the structure's natural frequencies, and TLCGD adjusts to these changes by controlling pressure drops in the diaphragm [12]. Lotfollahi-Yaghin identifies TLCGD as a cost-effective passive system, designed simply with sealed pipes connected to the main structure [40].

Experimental and numerical studies have been conducted to control vibrations exerted on foundations with a jacket. According to the literature, the best place to install the TLCGD damping system is at the top of a Jacket type offshore wind turbine. Such a structure is called JWOT [27]. There have been many studies on these structures, the best place to install the TLCGD system in JWOT, and the required properties [28, 40, 41]. Tuning the system involves adjusting the column lengths and gas pressure within vertical columns [30]. Jacket foundations, noted for their higher efficiency, cost-effectiveness, and simpler design, are among the best options for offshore wind turbines, though they have a lower natural frequency compared to other foundations [42]. The TLCGD system in these structures uses liquid to match the frequency with the natural frequency, offering superior flexibility. This setup allows the jacket foundation's velocity, movement, and acceleration to correspond with the movement of the liquid in the TLCGD [40]. Mousavi et al. further investigated this foundation type, evaluating its feasibility through specific equations [30].

According to the studies, although the JOWT foundation and TLCGD damper system are common and there is significant potential for offshore wind turbine installation in Iranian waters, no research has focused on optimal site selection under real wind and wave forces. This study uniquely uses meteorological and marine station data to conduct a feasibility analysis for turbine installation, applying dynamic behavior equations to identify the best locations based on the Power to Displacement Ratio (Rpd). By analyzing over 10,000 data points from the Caspian Sea, Oman Sea, and Persian Gulf, the study calculates optimal power and displacement values. The results, based on real data from the Iranian Oceanographic Center, are generalized to be applicable to other turbines.

2. Materials and Methods

This study assessed the feasibility of offshore wind turbine installation using a system combining a turbine, JOWT foundation, and TLCGD damping system. The design, informed by literature, embeds TLCGD within the foundation. The foundation's movement under wave and wind forces was analyzed, with equations linking this motion to the horizontal and vertical fluid movement within the TLCGD system.The system was modeled using a Multi-degree of Freedom (MDOF) approach, following the models proposed by Colwell et al. [12] and Lotfollahi et al. [40], and the dynamic equations were derived accordingly. These equations were solved using data from meteorological and marine stations, reflecting the structural characteristics of the studied system (Fig. 1). Twenty-six stations were selected based on oceanography research centers' data, providing suitable distances for analysis. The movement of the structure was

equated to the displacement of water in the U-section of the TLCGD and the average power output of the wind turbine. The study identified optimal locations for wind turbine installation.

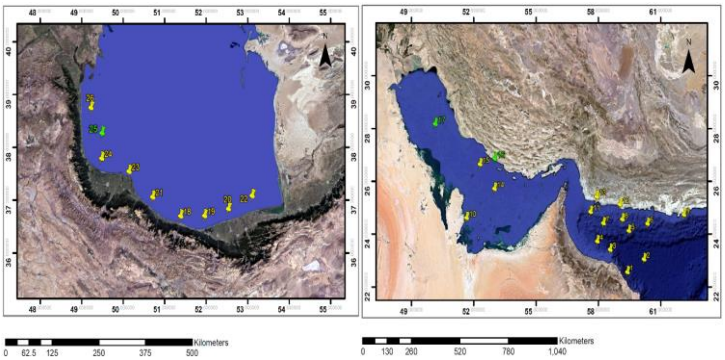

Fig. 1. Date station spots with databases to study the location

$$U = Z_a w e^{kz} cos(kx - wt) \quad (1)$$

$$W = Z_a w e^{kz} sin(kx - wt) \quad (2)$$

$$\dot{U} = Z_a w^2 e^{kz} sin(kx - wt) \quad (3)$$

$$\dot{W} = Z_a w^2 e^{kz} cos(kx - wt) \quad (4)$$

$$V = \sqrt{U^2 + W^2} \quad (5)$$

$$\dot{a} = \sqrt{\dot{U}^2 + \dot{W}^2} \quad (6)$$

where U denotes horizontal wave speed (m/s), W denotes vertical wave speed (m/s), V is total speed (m/s), a˙ denotes total acceleration (m/s²), Z_a is wave amplitude (m), w is angular frequency (rad/s), k is wavenumber (1/m), U˙ is horizontal wave acceleration (m/s²), and W˙ is vertical wave acceleration (m/s²).

2.1. Multi-degree of Freedom (MDOF) Model

In this article, based on the analysis of Mousavi et al. [30] and Colwell & Basu [12], the MDOF model is used to analyze the forces exerted on the system. As it is shown in Fig.2, the system was analyzed base on the Lotfollahi et al. [40] method in 5 degrees of freedom, and the related equations were extracted accordingly [12, 29].

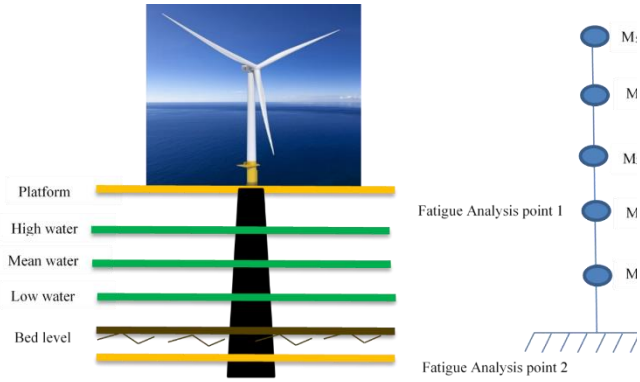

Fig. 2. Structural model for the jacket model for MDOF with 5 degrees of freedom

2.2. Dynamic Analysis of Forces Exerted on the Structure

The dynamic calculation using the Bernoulli equations extension would be obtained for the system displacement [8]. The turbine motion equations introduced to MATLAB, and then foundation and damper structure were developed and solved [43]. Under the wind wave effects, the dynamic behavior of wind turbines installed in offshore with jacket-type foundations can be explained as follows:

$$F_{Intertia} + F_{Damping} + F_{Elastic} = F_{Aaro} + F_{Hydro} \quad (7)$$

where the left side equation includes inertia, damping, and elastic forces, which are developed internally and formed in the turbine. Also, on the right side, the hydrodynamic and aerodynamic forces are external forces exerted on turbine and jacket-type structures [37].

2.2.1. Aerodynamic Force

In this study, the aerodynamic force, countered by thrust force, generates a plate-perpendicular force on the rotor due to the Yaw control mechanism. The impact of wind load on the tower and jacket foundation was deemed negligible and therefore not included in the analysis to simplify the research. Blade element momentum theory estimates drag and lift forces on blades. Based on classical BEM theory, these forces can be estimated by the following equations:

$$D = 0.5\rho_{air} V_{rel}^2 c C_d \quad (8)$$

$$L = 0.5\rho_{air} V_{rel}^2 c C_l \quad (9)$$

Here, L and D are lift and drag forces on the blade in terms of a length unit. Moreover, ρ_{air} denotes air density (kg/m³), c is chord length in the blade (m), and V_{rel} is the abbreviated form of wind relative velocity observed by the rotating blade (m/s). It is important to note that the relative velocity of wind results from axial wind velocity perpendicular to the rotor plate, angle velocity of the blade, and rotating flow around the blade based on wake rotation. Parameters C_d and C_l are drag and lift coefficients of blade, respectively. Thrust force dT increase in each blade element can be estimated as follows:

$$dT = F_N = L_b(D\,sin\,\varphi + L\,cos\,\varphi) \quad (10)$$

It is noticeable that element radial location of the blade is considered. The total thrust force can be estimated by the equation below:

$$F_{Aero} = T = B\sum_{i=1}^{n} dT_i \quad (11)$$

where B is the number of blades and n is the number of elements in each blade. Modifications to enhance aerodynamic load accuracy include adjusting for peak loss in pyrantel blades, Glart modification, wind-induced instability, and blade interactions like dynamic stall [37, 44].

2.2.2. Hydrodynamic Forces

Formulation to estimate the hydrodynamic forces exerted on the jacket-type foundation is taken as with JOWT, as follows [45]:

$$F_{Hydro} = F_D + F_I = 0.5\rho_w C_D A(v - \dot{u})|v - \dot{u}| + \rho_w B(C_M\dot{v} - (C_M - 1)\ddot{u}) \quad (12)$$

where F_{Hydro} denotes hydrodynamic vector, F_D and F_I are drag and inertia force vectors, respectively and ρ_w is water density (kg/m³). Matrices A and B are the area and volume matrices of the jacket, respectively (m² for area and m³ for volume). In addition, C_D and C_M

are drag and inertia coefficients of jacket elements (dimensionless). Moreover, v and $\dot{v}$ are velocity (m/s) and acceleration (m/s²) vectors, respectively. Finally, $\dot{u}$ is jacket absolute velocity (m/s) and $\ddot{u}$ is absolute acceleration (m/s²) [43].

2.2.3. Damper System (TLCGD)

TLCGD is a tunable system similar to the gas spring in line with fluid frequencies. Fig. 3 demonstrates TLCGD and its important parameters. The place of the damper system was considered inside the base of the jacket.

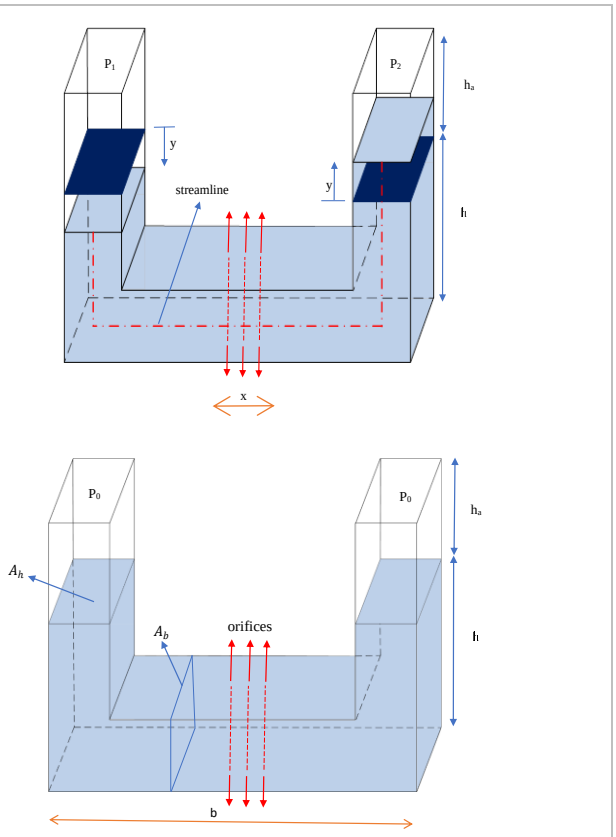

Fig. 3. TLCGD motion under the foundation X induction and related parameters [16]

3. Results

According to Mousavi et al [30], fluid motion in columns of TLCGD can be expressed as follows:

$$\ddot{y} + \delta_L|\dot{y}|\dot{y} + \omega_A^2 y = -k_1\ddot{x} \quad (13)$$

Where:

$$\omega_A^2 = \frac{2\left(1+\frac{nP_o}{\rho g h_a}\right)}{2h+b\lambda} \quad (14)$$

$$k_1 = \frac{b}{2h+b\lambda} \quad (15)$$

$$\lambda_L = \frac{1}{2(2h+b\lambda)}\left(K_{el}(1+\lambda^2) + N_b K_{or}\lambda^2 + N_h K_{or} + K_C + K_E + \frac{2fh}{D_h} + \frac{fb}{D_b}\lambda^2\right) \quad (16)$$

if λ is greater than 1, then $K_C = 0.5\lambda(\lambda\text{-}1)$ and $K_E = (\lambda\text{-}1)^2$. Also, if λ is greater than 1, then $K_C = 0.5(\lambda\text{-}1)$ and $K_E = (\lambda\text{-}1)^2$. Finally, if λ is equal to 1, then $K_C = K_E = 0$.

In these equations, x denotes the TLCGD horizontal foundation movement (m), and y is the fluid movement in vertical columns (m). The vertical and horizontal column lengths filled with fluid are h (m) and b (m). Moreover, A_b and A_h are horizontal and vertical column areas (m²), respectively. As shown in Fig. 3, h_a denotes vertical columns length filled with gas with primary pressure of P_0 (Pa). Fluid movement frequency, i.e., TLCGD frequency, is represented by W_A (rad/s) and TLCGD hydraulic head drop is denoted by δ_L (dimensionless). In addition, the parameter λ is the area ratio, i.e., the vertical column area to the horizontal column area (dimensionless). In addition, K_{el} and K_{or} are hydraulic head drop local coefficients for U-shaped joints and orifices, respectively (dimensionless). N_h and N_b are some orifices places in vertical and horizontal columns, respectively (dimensionless). D_h and D_b are vertical and horizontal column's diameters (m), respectively. K_C and K_E are contraction and expansion coefficients in vertical and horizontal columnar joints, respectively (dimensionless). Finally, f is the friction coefficient within the inner parts of vertical and horizontal columns (dimensionless). The TLCGD forces are obtained using the following equations [37].

$$F_1 = m_f\ddot{x} \quad (17)$$

$$F_2 = \rho b A_b \lambda\ddot{y} = \rho b A_h \ddot{y} \quad (18)$$

where F_1 is the internal force (N) and F_2 is the main controlling force (N) based on the fluid fuzzy external acceleration in the seismic form in horizontal columns of the TLCGD. Also, m_f and ρ are TLCGD fluid mass (kg) and fluid density (kg/m³), respectively. $\ddot{x}$ is absolute acceleration in the TLCGD foundation (m/s²). Along with some mathematical simplifications, the sum of TLCGD forces exerted on the structure is written as equations below:

$$F_{TLCGD} = m_f(\ddot{x} + k_{bar}\ddot{y}) \quad (19)$$

$$k_{bar} = \frac{b}{2h+\frac{b}{\lambda}} \quad (20)$$

Turbine power (P(W)) were calculated with equation (1) for each data in specific time and location [46]:

$$F_1 = m_f\ddot{x} \quad (21)$$

$$F_2 = \rho b A_b \lambda\ddot{y} = \rho b A_h \ddot{y} \quad (22)$$

In Betz's Law Wind Turbine Wind Power equation, P denotes turbine power (W), p denotes air density (kg/m³), A denotes sweap area (m²), V denotes wind total speed (m/s) and Cp is the power coefficient of the blades due to the Betz formula is 0.59 [45, 46]. The final simplified equation treats vertical fluid movement in TLCGD as a passive value, corresponding to the disk's vertical fluid movement.

The equations were solved using the "ode45" solver in MATLAB, providing the rate of horizontal fluid displacement in TLCGD relative to its vertical displacement. Diagrams were generated, and wind field speed was calculated using the wind turbine power formula. With

around 10,000 data points per day from 26 databases, mean values of U and P were calculated, and distances were determined using Euclidean geometry. MATLAB was used to identify optimal location points, achieving a 70% proximity to the ideal points.

The rated capacity of wind turbines is crucial for site selection, influencing both economic feasibility and energy yield. Higher capacities restrict sites to areas with stronger winds, while lower capacities offer more flexibility [47, 48]. The decision to focus on 6 MW offshore wind turbines in this article is strongly supported by comprehensive recent research [49, 50] which underscores their technological advancements [51] and suitability [52] for offshore energy production. The adoption of 6 MW offshore wind turbines is underscored in research due to their high energy yield [53] and operational efficiency in offshore environments. These types of turbines have been used by authors in various researches [50, 53]. These turbines are strategically placed to mitigate wake effects, enhancing efficiency and reducing operational costs [54]. They are also designed to endure marine conditions, offering longer operational life and significant environmental benefits due to their minimal landscape impact [55]. This aligns with global sustainability goals by balancing technological, economic, and societal factors. Notably, Chen and kim [56] have demonstrated through time-domain analysis that optimizing the structural design of these turbines significantly enhances their efficiency and sustainability. Furthermore, studies by Zheng and colleagues [53] on the hydrodynamic responses of spar-type floating offshore wind turbines confirm that 6 MW turbines perform exceptionally under various marine conditions, optimizing stability and power output. These references collectively justify the selection of 6 MW turbines for in-depth discussion, highlighting their role as a cornerstone in the future of renewable energy technologies.

A 6 MW turbine, fitting within the typical 4-15 MW offshore range [5], was selected for this study to balance energy yield and site flexibility, making it a reliable model for diverse site conditions. The selected wind turbine system, featuring a jacket, specific height, and internal TLCGD damper, was based on the specifications outlined in Table 1 [57].

$$m\ddot{u} + c\dot{u} + ku = B\sum_{i=1}^{n} L_b[(0.5\rho_{air}V_{rel}^2 cC_d)\sin\varphi + (0.5\rho_{air}V_{rel}^2 cC_d)\cos\varphi] + 0.5\rho_W C_D A[V-\dot{u}]|V-\dot{u}| + \rho_w B(C_M\dot{v} - (C_M-1)\ddot{u}) + m_f[\ddot{u} + K_{bar}\ddot{y}] \quad (23)$$

$$y = \ddot{y} + \delta_L|\dot{y}|\dot{y} + \omega_A^2 y = -K_1\ddot{u} \quad (24)$$

Table 1. Wind turbine geometric parameters

Element	Value
Nominal power of the turbine	6 MW
Blades	3 blades with a length of 50.0 m
Rotor diameter	100 m
Hub height	95 m
Wind nominal speed	4 m/s
Rotor nominal speed	6.2 RPM
Generator Efficiency	95.6%
Mass	400 tons
Cut-in wind speed	3 m/s
Cut-out wind speed	25 m/s

The power curve of a wind turbine is shown in Fig. 4.

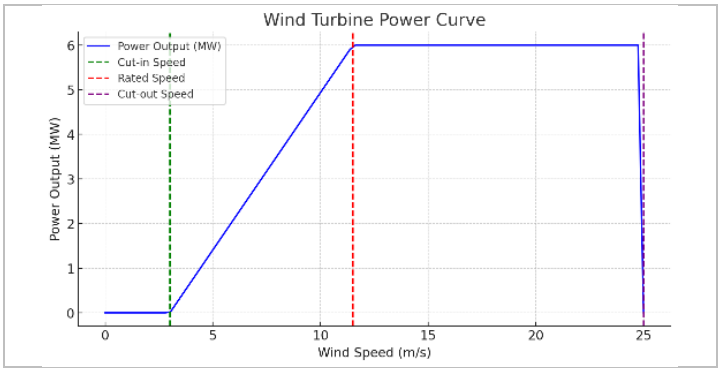

Fig. 4. Wind turbine's power curve

Geometric properties are presented in Table. 2. This jacket is investigated as a system and TLCGD's role in responding [29].

Table 2. Jacket geometric parameters [29, 38]

Size	Column	Pile	Beam	Brace
External diameter (m)	2.00	1.80	0.70	0.70
Internal diameter (m)	1.96	1.76	0.68	0.68

Foundation and damping system geometric parameters were extracted and listed in Table .3.

3. Results and Discussions

In this study, wind turbine efficiency and behavior were analyzed using meteorological, marine, and geological data, focusing on external forces such as wind, wave, hydrodynamic, and aerodynamic forces. A specific turbine structure with a jacket foundation was chosen based on existing literature for JWOT and TLCGD. The structure and damping column shapes were analyzed using the MDOF technique, and their dynamic formulas were derived. In the next stage, the structural movement *U* and turbine output power *P* were considered to estimate the suitable location for wind turbine installation with certain features.

The charts were prepared using MATLAB software based on the entire system displacement in terms of power. For example, Fig. 5 shows Point 25 with geographical coordinates of 38 N and 49.4 E. This point is predicted to be suitable for installing this type of wind turbine with a damping system. The chart was drawn using the wind and waves data. As can be seen, the maximum displacement and power are 48.7 cm and about 4.6 MW, respectively.

It is noteworthy that some points have higher power generation potential, although they cannot be the best choice as their displacements are in the highest range. The most suitable point should be the highest power generator with the least displacement. Nevertheless, considering the same analysis for a group of the points with less displacement cannot be a good option as the best location for

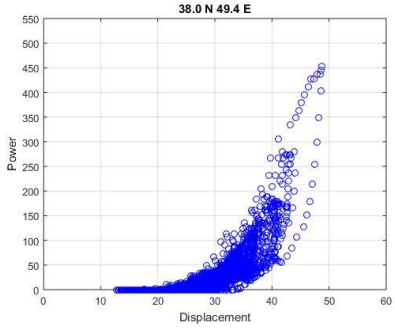

Fig. 5. A comparison of power and displacement data for point 25 (sample point)

installing the turbines because their power generation is not as high to be the most optimized one.

The Caspian Sea with 9 locating points, the Oman Sea with 5 locating points, and the Persian Gulf with 12 points (with suitable distances) were selected and coded in MATLAB for all 26 points. Based on MATLAB, the power diagram was extracted for 26 movement bases. As shown in Fig. 6. the power generation can be enhanced. This enhancement is accompanied by an increase in displacement *U*, which is dangerous for the installed platform. As shown in Fig. 6, the vertical column shows a power whose maximum level is 5.5 MW. The power generation is based on liquid horizontal movement in TLCGD, which is taken into account on the horizontal side of the diagram. As a result, the maximum movement value was obtained to be 60 cm. This maximum value of 56 cm occurred in several points, constituting the horizontal column.In Fig. 6, Points 14 and 15 placed in Persian Gulf have the maximum power generation, i.e., 5.5 MW, which is high and desirable power for wind turbines. However, because the vibrations to the system are high, 53.6 and 56.2 respectively, there are not suitable locations to install these turbines . In Points 18 and 19 located in Caspian Sea have have vibrations to the system and displacement reach 32.4 and 37.2 cm, which are suitable in terms of the health and stability of the structure. However, theses points are not desirable since the power output are 0.3 and 1.2 MW, which is not significant. Also Point 1 in Oman sea has a power production of 0.25 MW, which is very weak and non-optimize. The overall assessment suggests that the Oman Sea is generally not an ideal location for installing this type of wind turbine, with the exception of points 2 and 7, which demonstrated higher potential for electrical power generation and had acceptable displacement of less than 45 centimeters. In other areas, energy production was typically around 0.5 megawatts. At point 7, a maximum power output of 1.7 megawatts was observed, but this occurred infrequently. In contrast, the Persian Gulf, despite having fewer data points, was found to be a highly suitable region for energy production. As mentioned earlier, points 14 and 15, although capable of high power generation, experienced significant base displacement. However, points 16 and 17 were identified as optimal, producing mean 3 megawatts of power with displacements below 45 centimeters. The Caspian Sea also exhibited considerable potential for the installation of this type of wind turbine with a damper in most of the evaluated locations. Points 22, 25, and 26 were identified as the best sites, with estimated power outputs of approximately 3, 4, and 3 megawatts respectively, and displacements under 45 centimeters. Other locations, while showing low displacement, also had lower power generation capabilities.

The three points determined by MATLAB in terms of optimal distance were calculated so that 70% of the points were close to the center regarding displacement and power generation, and the three points obtained were considered the desired score.

Fig. 7 presents the power production capacity of the wind turbine system and the foundation displacement according to wind and wave data in specific databases for the Iran seas. In this study, both turbine production power range and foundation displacement were obtained in the Iran seas. Also, three points with optimal efficiency with the range of 70% less displacement and more power production capacity were obtained with MATLAB. The obtained results were selected according to the desired system but can be generalized to similar systems with different scales. The system used in the present study has the highest amount of power generation in the Persian Gulf compared to all other places in other Iran. However, despite the TLCGD dumping system considered in the JWOT base in the Persian Gulf, more than 55 cm of displacement was observed in the structure. Consequently, it will cause damage and reduce the efficiency of the wind turbine [61]. Besides, the fatigue life of structural fatigue will be reduced. The system can generate up to 5.5 MW of electrical power in these areas. Analyzed wave and wind data of existing bases, and the obtained results showed that the desired system in the western and northwestern regions of the Persian Gulf could produce suitable power between 3.5 to 4.5 MW. Also, the shaking and displacement of the system's foundation do not exceed 40 to 45 cm, and the system will function properly in the most optimal conditions. Accordingly, the structure will suffer less damage, have a longer lifespan, and have greater efficiency.

Corresponding contours for the Caspian Sea and the Persian Gulf are depicted in Fig. 8. Points 25, 17, and 16 in Hashtpar, Kish Island, and Bushehr bases are demonstrated as three suitable points for offshore wind turbine installation.

4. Conclusions

In this study, the feasibility of an offshore wind turbine with a jacket base and a TLCGD damping system was examined at 26 sites in the Caspian Sea, Persian Gulf, and Sea of Oman. Using MATLAB's ode45 solver, over 10,000 wind and wave measurements were analyzed. The study detailed the analysis of both vertical and horizontal wind motions, wave periods, and heights, alongside the impacts of hydrodynamic and aerodynamic forces on the system's displacement. It also explored the correlation between the horizontal and vertical movements of the damping system, estimating the vertical movement of P-U liquid based on horizontal shifts. Additionally, the power output of the turbine at each site was computed and the findings were mapped and evaluated using ArcGIS software.

According to the numerical and ArcGIS analysis results, the power generation capacity in the western and northwestern parts of the Caspian Sea is more appropriate and reaches 2.7 to 3.6 MW. In contrast, in the middle and northeastern parts, power generation was very low (i.e., about 1.8 to 2.3 MW). In the Caspian Sea, the highest output power of the wind turbine system was related to Point 25 with maximum value of 4.5 MW. Points 22 and 26 also reached the highest power of about 3.7 and 3.5 MW, respectively. The lowest displacement occurred at Points 18 and 19, with 32 and 37 cm, respectively. These points are located exactly in the middle of the Caspian Sea .

In the Oman Sea, the highest power output is related to Point 7 to the 1.7 MW with a displacement of 43 cm, located in the mid-western part of the Oman Sea. The system used in the current study has the highest amount of power generation in the Persian Gulf compared to all other places in other Iran. Moreover, most structural displacements were related to this sea. Point 16 (located in the coastal area and the surrounding area with an average power output of 4.2 MW and a displacement of 50 cm) and Point 17 (located in the west of the Persian Gulf with an average power generation of 3.9 MW and a displacement of 49 cm) were selected as suitable areas for installing these systems for energy generation. Finding the system structure displacement that causes the system to fail depends on the materials used in construction and other parameters. Therefore, in this article, this issue cannot be judged; however, it seems that areas with the ratio of power production capacity to their displacement between points 6 and 9 are suitable for installing these systems. Therefore, it can be stated that the area around Points 2 and 7 in the Oman Sea, around Points 10, 16, and 17 in the Persian Gulf, and around Points 22, 25, and 26 in the Caspian Sea are suitable locations for installing these power generation systems with offshore wind turbine and damper.

In conclusion, future research should enhance vibration absorbers, integrate active control systems, and conduct real-world testing. Additionally, it is recommended to incorporate seismic data, compare turbine sizes for optimal efficiency, and prioritize the use of durable, eco-friendly materials while managing environmental impacts.

References

[1] P. A. Østergaard, N. Duic, Y. Noorollahi, and S. A. Kalogirou, "Recent advances in renewable energy technology for the energy transition," vol. 179, ed: Elsevier, 2021, pp. 877-884.

[2] P. A. Østergaard, N. Duic, Y. Noorollahi, and S. Kalogirou, "Renewable energy for sustainable development," ed: Elsevier, 2022.

[3] X. Wu *et al.*, "Foundations of offshore wind turbines: A review," *Renewable and Sustainable Energy Reviews*, vol. 104, pp. 379-393, 2019.

[4] Y. Kumar *et al.*, "Wind energy: Trends and enabling technologies," *Renewable and Sustainable Energy Reviews*, vol. 53, pp. 209-224, 2016.

[5] G. W. E. Council, "Global offshore wind report 2020," *GWEC: Brussels, Belgium*, vol. 19, pp. 10-12, 2020.

[6] J. Luengo, V. Negro, J. García-Barba, J.-S. López-Gutiérrez, and M. D. Esteban, "New detected uncertainties in the design of foundations for offshore wind turbines," *Renewable Energy*, vol. 131, pp. 667-677, 2019.

[7] M. J. Dvorak, C. L. Archer, and M. Z. Jacobson, "California offshore wind energy potential ",*Renewable energy*, vol. 35, no. 6, pp. 1244-1254, 2010.

[8] N. Luo, L. Pacheco, Y. Vidal Seguí, and H. Li, "Smart structural control strategies for offshore wind power generation with floating wind turbines," in *Renewable energies & power quality journal (RE&PQJ), no. 10, 25th April 2012*, 2012 .

[9] G. Malliotakis, P. Alevras, and C. Baniotopoulos, "Recent advances in vibration control methods for wind turbine towers," *Energies*, vol. 14, no. 22, p. 7536, 2021.

[10] A. Nazokkar and R. Dezvareh, "Vibration control of floating offshore wind turbine using semi-active liquid column gas damper," *Ocean Engineering*, vol. 265, p. 112574, 2022.

[11] H. Peng, S. Li, L. Shangguan, Y. Fan, and H. Zhang, "Analysis of wind turbine equipment failure and intelligent operation and maintenance research," *Sustainability*, vol. 15, no. 10, p. 8333, 2023.

[12] S. Colwell and B. Basu, "Tuned liquid column dampers in offshore wind turbines for structural control," *Engineering Structures*, vol. 31, no. 2, pp. 358-368, 2009.

[13] L .Jin-Yang, Z. Songye, J. Zhang, M. Ruisheng, and Z. Haoran, "Vibration control of offshore wind turbines with a novel energy-adaptive self-powered active mass damper," *Engineering Structures*, vol. 302, p. 117450, 2024.

[14] A. Awada, R. Younes, and A. Ilinca, "Review of vibration control methods for wind turbines," *Energies*, vol. 14, no. 11, p. 3058, 2021.

[15] K. Sandal and V. Zania, "Optimization of pile design for offshore wind turbine jacket foundations," *OPTIMIZATION*, vol. 1000, p. 3, 2016.

[16] R .Dezvareh, K. Bargi, and S. A. Mousavi, "Control of wind/wave-induced vibrations of jacket-type offshore wind turbines through tuned liquid column gas dampers," *Structure and Infrastructure Engineering*, vol. 12, no. 3, pp. 312-326, 2016.

[17] T. Konar and A. Ghosh, "A review on various configurations of the passive tuned liquid damper," *Journal of Vibration and Control*, vol. 29, no. 9-10, pp. 1945-1980, 2023.

[18] S. Ahmad and S. Ahmad, "Active control of non-linearly coupled TLP response under wind and wave environments," *Computers & structures*, vol. 72, no. 6, pp. 735-747, 1999.

[19] M. A. Lackner and M. A. Rotea, "Passive structural control of offshore wind turbines," *Wind energy*, vol. 14, no. 3, pp. 373-388, 2011.

[20] M. A. Lackner and M. A. Rotea, "Structural control of floating wind turbines," *Mechatronics*, vol. 21, no. 4, pp. 704-719, 2011.

[21] M. L. Brodersen, A. S. Bjørke, and J. Høgsberg, "Active tuned mass damper for damping of offshore wind turbine vibrations," *Wind Energy*, vol. 20, no. 5, pp.2017 ,783-796 .

[22] Y. Wang, B. Li, X. Zhou, D. Zhu, and X. Huang, "Effectiveness of installing multiple tuned mass dampers for seismic mitigation of steel–concrete wind turbine hybrid tower," in *Structures*, 2024, vol. 60: Elsevier, p. 105838 .

[23] V .N. Dinh and B. Basu, "Passive control of floating offshore wind turbine nacelle and spar vibrations by multiple tuned mass dampers," *Structural Control and Health Monitoring*, vol. 22, no. 1, pp. 152-176, 2015.

[24] B. Zhao, H. Gao, Z. Wang, and Z. Lu, "Shaking table test on vibration control effects of a monopile offshore wind turbine with a tuned mass damper," *Wind energy*, vol. 21, no. 12, pp. 1309-1328, 2018.

[25] J. Zhang, X. Liang, L. Wang, B. Wang, and L. Wang, "The influence of tuned mass dampers on vibration control of monopile offshore wind turbines under wind-wave loadings," *Ocean Engineering*, vol. 278, p. 114394, 2023.

[26] H. Zhang *et al.*, "Experimental study on mitigating vibration of floating offshore wind turbine using tuned mass damper," *Ocean Engineering*, vol. 288, p. 115974, 2023.

[27] Q. Jin, X. Li, N. Sun, J. Zhou, and J. Guan, "Experimental and numerical study on tuned liquid dampers for controlling earthquake response of jacket offshore platform," *Marine Structures*, vol. 20, no. 4, pp.2007 ,238-254 .

[28] M. J. Hochrainer and F. Ziegler, "Control of tall building vibrations by sealed tuned liquid column dampers," *Structural Control and Health Monitoring: The Official Journal of the International Association for Structural Control and Monitoring and of the European Association for the Control of Structures*, vol. 13, no. 6, pp. 980-1002, 2006.

[29] S. A. Mousavi, S. M. Zahrai, and K. Bargi, "Optimum geometry of tuned liquid column-gas damper for control of offshore jacket platform vibrations under seismic excitation," *Earthquake Engineering and Engineering Vibration*, vol. 11, no. 4, pp. 579-592, 2012.

[30] S. A. Mousavi, K. Bargi, and S. M. Zahrai, "Optimum parameters of tuned liquid column–gas damper for mitigation of seismic-induced vibrations of offshore jacket platforms," *Structural Control and Health Monitoring*, vol. 20, no. 3, pp. 422-444, 2013.

[31] C. Coudurier, O. Lepreux, and N. Petit, "Modelling of a tuned liquid multi-column damper. Application to floating wind turbine for improved robustness against wave incidence," *Ocean Engineering*, vol. 165, pp. 277-292, 2018.

[32] T. Balendra, C. Wang, and H. Cheong, "Effectiveness of tuned liquid column dampers for vibration control of towers," *Engineering Structures*, vol. 17, no. 9, pp. 668-675, 1995.

[33] H. Gao, K. Kwok, and B. Samali, "Optimization of tuned liquid column dampers," *Engineering structures*, vol. 19, no. 6, pp. 476-486, 1997.

[34] J. K. Vandiver and S. Mitome, "The effect of liquid storage tanks on the dynamic response of offshore platforms," *Journal of Petroleum Technology*, vol. 31, no. 10, pp. 1231-1240, 1979.

[35] K. Yamamoto and M. Kawahara, "Structural oscillation control using tuned liquid damper," *Computers & structures*, vol. 71, no. 4, pp. 435-446, 1999.

[36] S .K. Yalla and A. Kareem, "Optimum absorber parameters for tuned liquid column dampers," *Journal of Structural Engineering*, vol. 126, no. 8, pp. 906-915, 2000.

[37] K. Bargi, R. Dezvareh, and S. A. Mousavi, "Contribution of tuned liquid column gas dampers to the performance of offshore wind turbines under wind, wave, and seismic excitations," *Earthquake Engineering and Engineering Vibration*, vol. 15, no. 3, pp. 551-561, 2016.

[38] P. Sathish and A. Sajith, "Study of Offshore Jacket Platform Attached With Tuned Liquid Column Gas Damper," in *International Conference on Offshore Mechanics and Arctic Engineering*, 2017, vol. 57632: American Society of Mechanical Engineers, p. V001T01A067 .

[39] M. H. Jahangir, S. A. Mousavi, and M. A. V. Rad, "A techno-economic comparison of a photovoltaic/thermal organic Rankine cycle with several renewable hybrid systems for a residential area in Rayen, Iran," *Energy Conversion and Management*, vol. 195, pp. 244-261, 2019.

[40] M. A. Lotfollahi-Yaghin, H. Ahmadi, and H. Tafakhor, "Seismic responses of an offshore jacket-type platform incorporated with tuned liquid dampers," *Advances in Structural Engineering*, vol. 19, no. 2, pp. 227-238, 2016.

[41] F. Ziegler, "Special design of tuned liquid column-gas dampers for the control of spatial structural vibrations," *Acta Mechanica*, vol. 201, no. 1-4, pp. 249-267, 2008.

[42] D. K. Kwon, A. Kareem, and K. Butler, "Gust-front loading effects on wind turbine tower systems," *Journal of wind engineering and industrial aerodynamics*, vol ,104 .pp. 109-115, 2012.

[43] P. Sathish and A. Sajith, "Study of Offshore Jacket Platform Attached With Tuned Liquid Column Gas Damper," in *ASME 2017 36th International Conference on Ocean, Offshore and Arctic Engineering*, 2017: American Society of Mechanical Engineers Digital Collection .

[44] M. O. Hansen, "Aerodynamics of wind turbines. Earthscan," *James & James*, vol. 8, no. 9, p. 14, 2008.

[45] E. J. Laya, J. J. Connor, and S. S. Sunder, "Hydrodynamic forces on flexible offshore structures," *Journal of engineering mechanics*, vol. 110, no. 3, pp. 433-448, 1984.

[46] G. Amirinia, B. Kamranzad, and S. Mafi, "Wind and wave energy potential in southern Caspian Sea using uncertainty analysis," *Energy*, vol. 120, pp. 332-345, 2017.

[47] J. F. Manwell, J. G. McGowan, and A. L. Rogers, *Wind energy explained: theory, design and application*. John Wiley & Sons, 2010.

[48] Y. Yan, Y. Yang, M. Bashir, C. Li, and J. Wang, "Dynamic analysis of 10 MW offshore wind turbines with different support structures subjected to earthquake loadings," *Renewable Energy*, vol. 193, pp. 758-777, 2022.

[49] L. Meng, Y.-p. He, Y.-d. Liu, Y.-s. Zhao, and L. Yu, "Numerical study on influence of turbulent and steady winds on coupled dynamic response of 6-MW Spar-type FOWT," in *ISOPE International Ocean and Polar Engineering Conference*, 2018: ISOPE, pp. ISOPE-I-18-025 .

[50] L. Meng, T. Zhou, Y.-p. He, Y.-s. Zhao, and Y.-d. Liu, "Concept design and coupled dynamic response analysis on 6-MW Spar-type floating offshore wind turbine," *China Ocean Engineering*, vol. 31, pp. 567-577, 2017.

[51] L. Meng *et al.*, "Dynamic response of 6MW spar type floating offshore wind turbine by experiment and numerical analyses," *China Ocean Engineering*, vol. 34, no. 5, pp. 608-620, 2020.

[52] S.-H. Ju, Y.-C. Huang, and Y.-Y. Huang, "Study of optimal large-scale offshore wind turbines," *Renewable Energy*, vol. 154, pp. 161-174, 2020.

[53] Z. Zheng, J. Chen, H. Liang, Y. Zhao, and Y. Shao, "Hydrodynamic responses of a 6 MW spar-type floating offshore wind turbine in regular waves and uniform current," *Fluids*, vol. 5, no. 4, p. 187, 2020.

[54] N. J. Choi, S. H. Nam, J. H. Jeong, and K. C. Kim, "CFD study on aerodynamic power output changes with inter-turbine spacing variation for a 6 mw offshore wind farm," *Energies*, vol. 7, no. 11, pp. 7483-7498, 2014.

[55] J. Żywicki, P. Dymarski, E. Ciba, and C. Dymarski, "Design of structure of Tension Leg Platform for 6 MW offshore wind turbine based on FEM analysis," *Polish Maritime Research*, pp. 230-241, 2017.

[56] J. Chen and M.-H. Kim, "Review of recent offshore wind turbine research and optimization methodologies in their design," *Journal of Marine Science and Engineering*, vol. 10, no. 1, p. 28, 2022.

[57] J. Köller, J. Köppel, and W. Peters, *Offshore wind energy: research on environmental impacts*. Springer Science & Business Media, 2006.

[58] M. Hochrainer and P. Fotiu, "Design of coupled tuned liquid column gas dampers for multi-mode reduction in vibrating structures," *Acta Mechanica*, vol. 229, no. 2, pp. 911-928, 2018.

[59] F. Petrini, H. Li, and F. Bontempi, "Basis of design and numerical modeling of offshore wind turbines," *Structural engineering & mechanics*, vol. 36, no. 5, p. 599, 2010.

[60] H. Hokmabady, S. Mohammadyzadeh, and A. Mojtahedi, "Suppressing structural vibration of a jacket-type platform employing a novel Magneto-Rheological Tuned Liquid Column Gas Damper (MR-TLCGD)," *Ocean Engineering*, vol. 180, pp. 60-70, 2019.

[61] G. P. Corten and H. F. Veldkamp, "Insects can halve wind-turbine power," *Nature*, vol ,412 .no. 6842, pp. 41-42, 2001.

[62] B. Kamranzad, "Persian Gulf zone classification based on the wind and wave climate variability," *Ocean Engineering*, vol. 169, pp. 604-635, 2018.

[63] G. Amirinia, S. Mafi, and S. Mazaheri, "Offshore wind resource assessment of Persian Gulf using uncertainty analysis and GIS," *Renewable Energy*, vol. 113, pp. 915-929, 2017.

[64] B. Kamranzad, A. Etemad-Shahidi, and V. Chegini, "Assessment of wave energy variation in the Persian Gulf," *Ocean Engineering*, vol. 70, pp. 72.2013 ,80-

[65] A. Saket and A. Etemad-Shahidi, "Wave energy potential along the northern coasts of the Gulf of Oman, Iran," *Renewable Energy*, vol. 40, no. 1, pp. 90-97, 2012.

[66] M. Rahime, M. Gholamalifard, and A. R. E. Hesari, "Modelling the temporal and spatial wind energy trend in the Caspian Sea," 2020.

Table 3. Foundation and damping system geometric parameters.

Element	Value
Mass matrix (M) model as the sum of structural and additional masses *[38]*	$M = \begin{bmatrix} 157 & 0 & 0 & 0 & 0 \\ 0 & 154 & 0 & 0 & 0 \\ 0 & 0 & 151 & 0 & 0 \\ 0 & 0 & 0 & 137 & 0 \\ 0 & 0 & 0 & 0 & 1087 \end{bmatrix}$ ×1000 Kg
Hardness matrix (K) *[29, 38]*	$K = \begin{bmatrix} 1 & -0.444 & 0 & 0 & 0 \\ -0.444 & 0.819 & -0.375 & 0 & 0 \\ 0 & -0.375 & 0.661 & 0.286 & 0 \\ 0 & 0 & -0.286 & 0.353 & -0.067 \\ 0 & 0 & 0 & -0.067 & 0.067 \end{bmatrix}$ × 109 N/m
Mass and hardness suitable driver matrix (C) based on Rayleigh driver *[38]*	$C = \begin{bmatrix} 100 & -44.4 & 0 & 0 & 0 \\ -44.4 & 81.94 & -37.5 & 0 & 0 \\ 0 & -37.5 & 66.14 & 28.6 & 0 \\ 0 & 0 & -28.6 & 35.33 & -6.7 \\ 0 & 0 & 0 & -6.7 & 6.95 \end{bmatrix}$ ×107 N.s/m
Bending ratio for all states *[37]*	2%
Frequency of damper for 0.2 MPa *[38]*	4.94 rad/sec
The natural frequency of the structure *[38]*	5.94 rad/sec
Time period (T) *[38]*	10 sec
Wave height (H) *[38]*	1 unit
δ_L *[29, 37]*	0.5
i *[37]*	1
k_1 *[58]*	1.2
W_A *[58]*	7.15
D_L *[59]*	0.5
K_{bar} *[37]*	0.68
M_f *[58]*	0.274
B *[29]s*	[258 253 248 1770 0]
A *[29]*	[294 289 282 202 0]
C_m *[60]*	0.9
C_d *[60]*	0.9
P_w *[29]*	1000

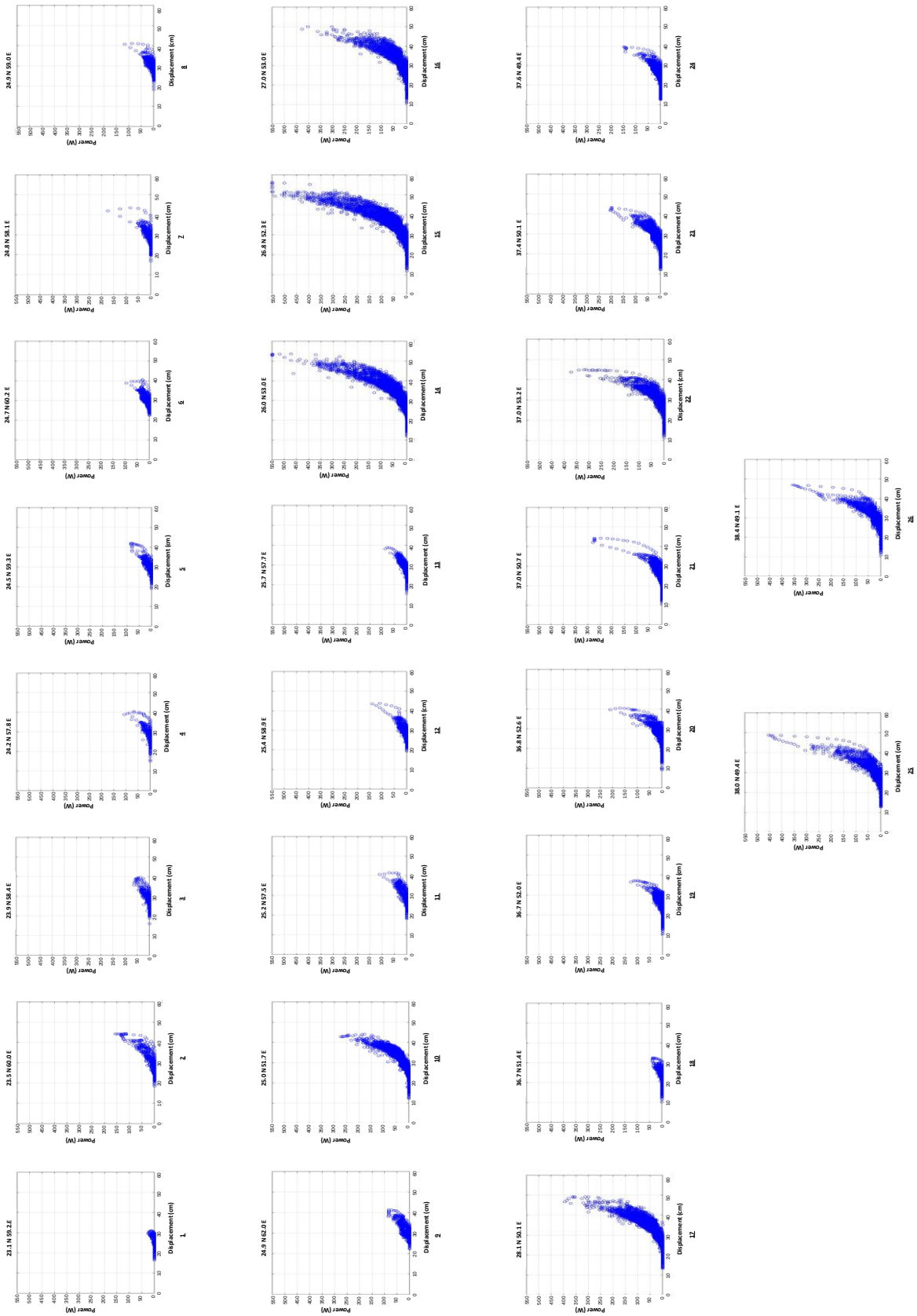

Fig. 6. Power versus displacement diagram for the selected areas by MATLAB

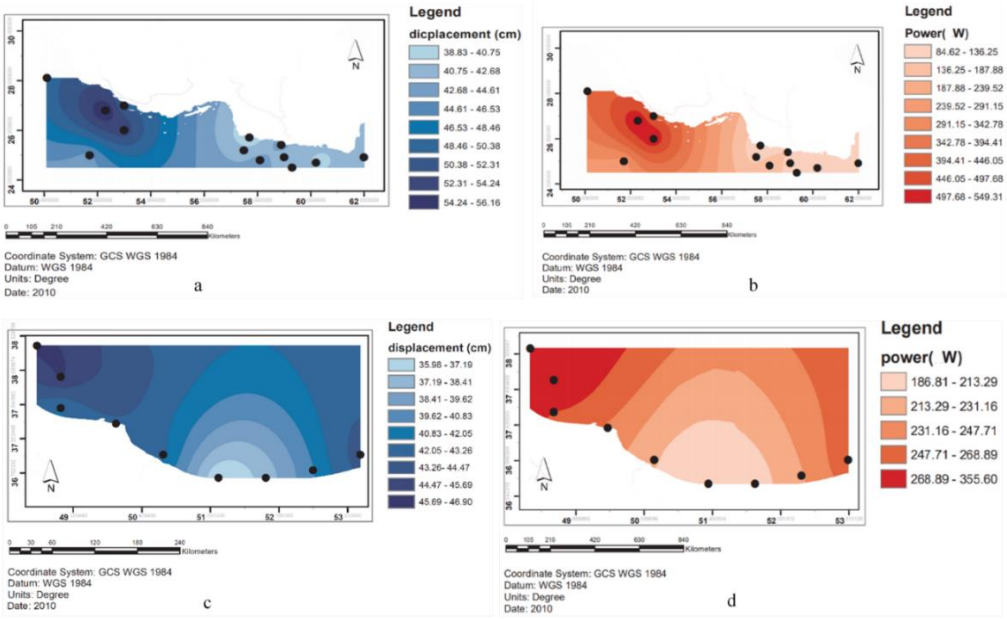

Fig. 7. Displacement and power contour of wind turbine installation in Iran, a) Caspian Sea Displacement Contour, b) Persian Gulf Displacement Contour, c) Caspian Sea Power Contour, and d) Persian Gulf Power Contour

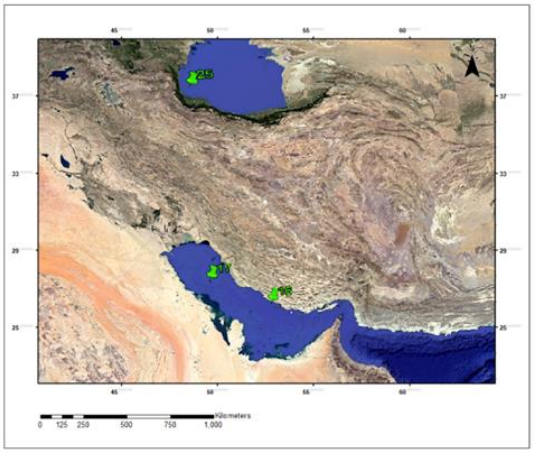

Fig. 8. Three desirable locations for off-shore wind turbine installation in Iran

Table 4. Spot locations in the Persian Gulf with databases to study the location and its date result

No	Locations		Max. power generated (kW)	Max. structure movement (cm)	Power to displacement ratio (kW/cm)
	Latitude	Longitude			
10	25.0 N	51.7 E	2729	44	62.02
14	26.0 N	53.0 E	5500	53.6	102.61
15	26.8 N	52.3 E	5500	56.2	97.87
16*	27.0 N	53.0 E	4276	50	85.52
17*	28.1 N	50.1 E	3945	49.1	80.35

* specified optimal points

Table 5. Spot locations in the Oman sea with databases to study the location and its date result

No	Locations		Max. power generated (kW)	Max. structure movement (cm)	Power to displacement ratio(kW/cm)
	Latitude	Longitude			
1	23.1 N	59.2 E	253	40	06.33
2*	23.5 N	60.0 E	1565	44.3	35.33
3	23.9 N	58.4 E	636	39.5	16.11
4	24.2 N	57.8 E	1065	40.4	26.37
5	24.5 N	59.3 E	846	42	20.15
6	24.7 N	60.2 E	936	40.4	23.17
7*	24.8 N	58.1 E	1745	43.4	40.21
8	24.9 N	59.0 E	1169	41.1	28.45
9	24.9 N	62.0 E	846	41.4	20.44
11	25.2 N	57.5 E	1099	41.5	26.49
12	25.4 N	58.9 E	1397	43.7	31.97
13	25.7 N	57.7 E	876	38.8	22.58

* specified optimal points

Table 6. Spot locations in the Caspian Sea with databases to study the location and its date result

No	Locations		Max. power generated (kW)	Max. structure movement (cm)	Power to displacement ratio (kW/cm)
	Latitude	Longitude			
18	36.7 N	51.4 E	374	32.4	11.54
19	36.7 N	52.0 E	1280	37.2	34.41
20	36.8 N	52.6 E	2093	40.4	51.81
21	37.0 N	50.7 E	2792	44.3	63.02
22*	37.0 N	53.2 E	3709	45	82.42
23	37.4 N	50.1 E	2041	43.1	49.68
24	37.6 N	49.4 E	1479	39.5	37.44
25*	38.0 N	49.4 E	4536	48.7	93.14
26*	38.4 N	49.1 E	3556	46.9	75.82

* specified optimal points